Design and Analysis of a Through-body Signal Transmission System based on Human Oxygen Saturation Detection

Chengyi Zhang, *Graduate Student Member, IEEE,* Hao Yan, *Member, IEEE,* Qiang Liu, *Member, IEEE,* Kun Yang, *Fellow, IEEE,* Fuqiang Liu, *Member, IEEE,* and Lin Lin, *Senior Member, IEEE*

***Abstract*—For a long time, people have carried out various studies on molecular communication (MC) and the Internet of Bio-Nanothings (IoBNT) in order to realize biomedical applications inside the human body. However, how to realize the communication between these applications and the outside body has become a new problem. In general, different components in the blood have different light absorption rates. Based on this, we propose a new through-body communication method. The nanomachine in the blood vessel transmits signals by releasing certain substances that can influence blood oxygen saturation. The change in blood oxygen saturation can be detected by an outside body device measuring the attenuation of the light through the blood. The framework of the entire communication system is proposed and mathematically modeled. Its error performance is discussed and evaluated. The mutual information (MI) of the designed communication system is also derived and calculated. This research will contribute to the realization of the connection of the IoBNT inside the human body to the outside device.**

***Index Terms*—molecular communication, nanomachine, oxygen saturation, light absorption, mutual information.**

I. Introduction

In recent years, the Internet of Bio-Nanothings (IoBNT) which envisages interaction between biological cells or nano-devices and the Internet has become a research hotspot [1]–[3]. The main goal of this emerging network framework is to enable direct and seamless interaction with biological systems in order to accurately sense and control their dynamics in real time. In the health monitoring application of IoBNT, nanomachines need to transmit data outside the human body from biosensors in the human body regarding the health status and vital signs of the human body. Similarly, in the disease prevention application, when sensors identify biomarkers, the nanomachines in IoBNT could send a signal to external devices for early diagnosis and intervention. So far, how to design a suitable interface for information transfer between nanomachines inside the human body and outside the human body remains an open research question in the field of IoBNT.

This problem has been explored by many different researchers from different fields. In [4], the authors proposed an ultra-low-power intra-body communication approach by implementing a galvanic impulse method for communication between an implant and an on-body device. An experimental study based on functional electrical stimulation with the human body as a communication channel was proposed by authors in [5]. In [6], the authors considered a neural communication approach to address this issue. Nanomachines were deployed in the human body and send signals by stimulating nerve fibers through electrodes. This signal propagated through the nerves and produced a surface electromyography signal, which serves as the information received by the body surface receiver. However, the signal transmission through the nervous system is susceptible to the interference of the action caused by the subjective consciousness of the human body on the neural signal reception.

Molecular communication is one of the very promising communication schemes for building the IoBNT, which enables communication between nano-devices in the human body [7], [8]. Combining molecular communication with some in-vitro detection methods enables the transfer of information from inside to outside the body. Thus many researchers tried to solve this problem with molecular communication methods. Some researchers considered using different kinds of nanoparticles like fluorescent nanoparticles [9] and metallic nanoparticles [10] as communication bridges. Information transfer between inside and outside the body through the use of molecules that can be selectively detected by in-vitro receivers. Some other researchers considered nanomachines and smart probes to solve this problem [11], [12]. In [13], the authors proposed to use smart probes fixed in blood vessels to release substances that will cause allergic reactions on the skin surface, so as to realize the interaction between the inside and outside of the human body. The probes were expected to release a substance that generates an allergic reaction on the skin surface or is detectable in the infrared bandwidth

This work was supported in part by the National Natural Science Foundation, China, under Grant 62371345, 61971314, 62071297; in part by the Fundamental Research Funds for the Central Universities under Grant 22120220629; in part by the Science and Technology Commission of Shanghai Municipality, under Grant 19510744900; and in part by the Sino-German Center of Intelligent Systems, Tongji University. (Corresponding author: Lin Lin and Fuqiang Liu.)

C. Zhang, F. Liu, and L. Lin are with the College of Electronics and Information Engineering, Tongji University, Shanghai 201804, China (e-mail: flyer@tongji.edu.cn; liufuqiang@tongji.edu.cn; fxlinlin@tongji.edu.cn).

H. Yan is with the School of Electronic, Information and Electrical Engineering, Shanghai Jiao Tong University, Shanghai 200240, China (e-mail: yan_hao@sjtu.edu.cn).

Q. Liu is with the School of Information and Communication Engineering, University of Electronic Science and Technology of China, Chengdu, Sichuan 611731, China (e-mail: liuqiang@uestc.edu.cn).

K. Yang is with the School of Computer Science and Electronic Engineering, University of Essex, Colchester CO4 3SQ, U.K. (e-mail: kunyang@essex.ac.uk).

F. Liu is also with the College of Design and Innovation, Tongji University, Shanghai 201804, China.

or by ultrasound. However, the authors did not elaborate on how to implement these ideas. The authors in [14] proposed an experimental platform for MC based on light absorption, providing experimental support for the design of molecular communication systems based on optical principles.

Our solution to this problem is inspired by the oximeter. A pulse oximeter is a portable and noninvasive tool widely used in clinical practice to evaluate the oxygenation status of a patient by monitoring arterial oxygen saturation [15]. We notice that the oximeter is often used outside the human body to detect the blood oxygen saturation in blood vessels. We can utilize this technique to realize the communication system through the human body. Blood oxygen saturation is one of the important basic data in clinical medicine, which can be inferred by measuring the attenuation of different light through blood [16]. The signal transmission through the body can be achieved by altering blood oxygen saturation and detecting its change outside the human body by optical method. The optical detection method based on blood oxygen saturation measurement is quite mature and has strong feasibility [17], but the idea of applying it to communication inside and outside the human body is still proposed for the first time. We presented the initial system framework in [18]. The main contributions of this paper are:

1) We propose a new through-body communication method that people can make use of blood oxygen saturation detection. The framework of the entire communication system is presented.

2) Our proposed system is mathematically modeled and the error performance is evaluated.

3) We use the knowledge of information theory to analyze and calculate the mutual information (MI) of the proposed system and evaluate various key parameters.

The rest of this paper is organized as follows. Section II introduces preliminary knowledge of optical technology and oxygen saturation and the design of our through-body communication system. Section III presents the mathematical model of our system. Section IV derives the MI for our system. Section V presents the simulation results. Section VI concludes the paper.

II. Design of Through-Body Communication System

In this section, we first explain the concept of blood oxygen saturation and the principle of its optical detection. After that, we present the design of the through-body communication system.

A. Blood Oxygen Saturation

The oxygen consumed by the human body mainly comes from the oxygen carried by hemoglobin. Hemoglobin is the protein contained in red blood cells that is responsible for the delivery of oxygen to the tissues. There are four kinds of hemoglobin in normal blood: oxygenated hemoglobin (HbO_2), deoxyhemoglobin (Hb), carboxyhemoglobin (COHb), and methemoglobin (MetHb). Among them, Hb and HbO_2 are reversibly combined with oxygen, while COHb and MetHb are not combined with oxygen. The function of hemoglobin is to carry oxygen to all parts of the body. The oxygen content of hemoglobin at any time is called blood oxygen saturation (S_{O_2}). S_{O_2} is used to describe the change of oxygen content in blood. It refers to the percentage of bound oxygen volume in total blood volume. When characterizing S_{O_2}, only the two functional hemoglobins of HbO_2 and Hb are considered [19]. COHb, MetHb, and other non-functioning hemoglobins are usually not considered. S_{O_2} can be expressed as [19]

$$S_{O_2} = \frac{C_{HbO_2}}{(C_{HbO_2} + C_{Hb})}. \tag{1}$$

The oxyhemoglobin dissociation curve also called the oxygen dissociation curve (ODC), is a curve that plots the proportion of hemoglobin in its saturated (oxygen-laden) form on the vertical axis against the prevailing oxygen tension on the horizontal axis. This curve is an important tool for understanding how our blood carries and releases oxygen. Specifically, the oxyhemoglobin dissociation curve relates oxygen saturation and partial pressure of oxygen in the blood (P_{O_2}) [20]. The hemoglobin oxygen dissociation curve is altered by changes in pH, temperature, and the red cell concentration of 2,3 diphosphate glyceride (2,3-DPG) [21].

B. Principle of Optical Detection

Photoplethysmography is a noninvasive optical technique widely used in the study and monitoring of the pulsations associated with changes in blood volume [22]. This technology is used in the optical detection method of the oximeter. As we mentioned before, HbO_2 is in the oxygen-carrying state and Hb is in the no-carrying state. HbO_2 and Hb have different absorption characteristics in the spectrum range of visible light and near-infrared. Hb absorbs more red-frequency light and less infrared-frequency light. HbO_2 absorbs less red frequency light and more infrared frequency light. The principle of a fingertip pulse oximeter is based on this fact [23]. When red light and infrared light irradiate the finger alternately, the photodiode in the fingertip pulse oximeter will produce a weak photocurrent that changes with the pulse. After converting, filtering, and amplifying the photocurrent, the pulse waveform is obtained. The pulse frequency is calculated from the peak spacing, and the blood oxygen saturation is calculated from the photocurrent ratio of red light and infrared light.

According to [24], when light of a specific wavelength is incident on the fingertip, the transmitted light intensity can be divided into two parts: the pulsatile component and the non-pulsatile component in the fingertip tissue. When the arterial blood vessels in the light-transmitting area pulsate, the amount of light absorbed by the arterial blood will change accordingly, which is called the alternating current (AC) component. The absorption of light by other tissues such as skin, muscle, bone, and venous blood is constant and is called the direct current (DC) component. If the attenuation due to factors such as scattering and reflection is ignored and according to the Lambert-Beer law, when the wavelength is λ and the

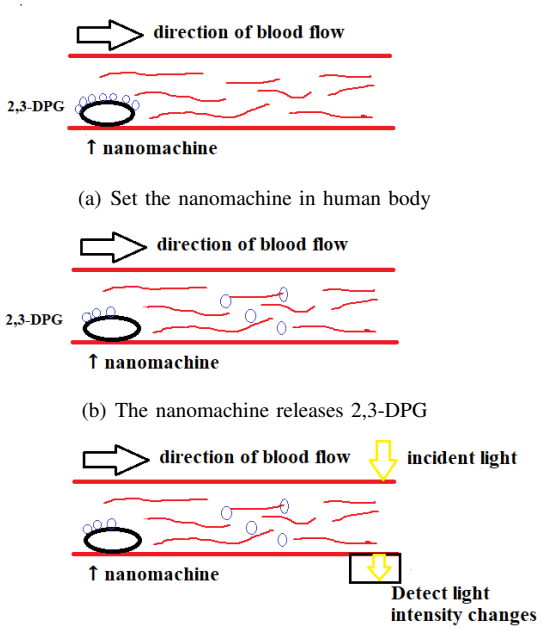

(a) Set the nanomachine in human body

(b) The nanomachine releases 2,3-DPG

(c) Detect light intensity changes

Fig. 1. The data transmission via human oxygen saturation detection.

monochromatic light with the light intensity of I_0 is vertically incident, the transmitted light intensity can be written as [25]

$$I = I_0 e^{-\varepsilon_0 C_0 L} e^{-\varepsilon_{HbO_2} C_{HbO_2} L} e^{-\varepsilon_{Hb} C_{Hb} L}, \tag{2}$$

where ε_0, C_0, L are the absorption coefficient, the concentration of light-absorbing substances, and the optical path length of non-arterial components in the tissue and venous blood. C_{HbO_2}, ε_{HbO_2} are the absorption concentration and coefficient of HbO_2 in arterial blood. C_{Hb} and ε_{Hb} are the absorption concentration and coefficient of Hb in arterial blood.

C. Through-Body Communication System Design

In order to achieve a feasible change of blood oxygen saturation in the blood vessel and make decisions based on the received light intensity at the receiving end, the nanomachine needs to release something to change the affinity of hemoglobin for oxygen. According to [26], CO_2 concentration, pH value, temperature, and 2,3-DPG all affect the affinity of hemoglobin for oxygen, thus causing changes in blood oxygen saturation. For safety and practical considerations, the pH value and temperature in human blood vessels cannot be easily changed, and CO_2 is unable to be carried by nanomachine as a gas molecule, so we consider that 2,3-DPG is used to change blood oxygen saturation.

The oxyhemoglobin dissociation curve shifts to the right with the increase of 2,3-DPG [27], which also represents the decrease in blood oxygen saturation. Due to the fast blood flow, the time for 2,3-DPG molecules to travel from the nanomachine to the receiver in our system is very short, and we can consider that the changes in blood oxygen saturation caused by changes in 2,3-DPG are much faster than regular natural saturation changes. The basic idea of our system design is that the nanomachine releases 2,3-DPG to change the blood oxygen concentration, thereby producing a change in the light intensity at the receiver and realizing the decision judgment. The whole process is shown in Fig. 1.

In fact, the role of 2,3-DPG on Hb binding and O_2 release is more complex [28]. Further studies are needed to determine the effect of controlling 2,3-DPG on changes in oxygen saturation, as it is not clear whether other tissue or cellular changes are induced during 2,3-DPG release and affect changes in blood oxygen levels. However, this is beyond the scope of this article, so it will not be discussed further here.

III. Mathematical Modeling of Designed Communication System

In this section, the mathematical modeling of the entire communication process from the nanomachine in the human body to the outside-body processing unit is presented.

The general idea is that 1) the nanomachine is deployed at the upstream fingertips of the human body to release the 2,3-DPG when it needs to send signals, and 2) we use a device that makes an optical measurement of blood oxygen saturation at the downstream fingertips. In this way, the data transmission from the nanomachine to the outside body device can be realized.

In a MC system, if the nanomachine transmits a bit $a \in \{0, 1\}$ to the outside of the human body, the nanomachine will release a certain amount of 2,3-DPG, which may be set as A molecules as

$$A = \begin{cases} M, a = 1 \\ 0, a = 0. \end{cases} \tag{3}$$

where M is the number of released molecules when bit "1" is transmitted.

So the concentration of the released information molecule at the transmitter can be expressed as

$$s(t) = \sum_{j=0}^{\infty} A_j \delta(t - jT), \tag{4}$$

where A_j is the number of the released molecules for the jth symbol and T is the symbol interval.

Next, in order to simplify the problem, we first consider that 2,3-DPG molecules move with blood flow. The diameter of a 2,3-DPG molecule is much less than the diameter of the transverse palmar branch since the volume of 2,3-DPG is around 10^{-19} mm^3 and the diameter of blood vessels in fingers is up to 1.5 mm [29]. In the case of limited transmission distance, we can regard the process of 2,3-DPG molecular transmission in fingertip vessels as a borderless system. We adopt a model in [30] for 3-D advection-diffusion where the channel impulse response (CIR) was obtained as

$$h(t) = \frac{1}{(4\pi D t)^{\frac{3}{2}}} e^{-\frac{(d-vt)^2}{4Dt}}, \tag{5}$$

where v is the average speed of the blood flow, and d is the distance between the nanomachine and the receiver. D is the diffusion coefficient for 2,3-DPG molecules in blood vessel.

Based on the principle of communication, the output signal is equal to the convolution of the input signal with the

CIR. Thus, the molecular concentration $y(t)$ after propagation through the blood vessel via diffusion is given by

$$\begin{aligned} y(t) &= s(t) * h(t) \\ &= \sum_{j=0}^{\infty} A_j h(t - jT), \quad j = 0, 1, \ldots, \end{aligned} \tag{6}$$

where * denotes the convolution operator.

Here $y(t)$ can be further split into the sum of the molecular concentration of the jth signal and the inter-symbol interference(ISI) signal and expressed as

$$y(t) = C_j(t) + z_{\mathrm{ISI},j}(t), \tag{7}$$

where $C_j(t)$ is the received molecular concentration of the current jth symbol and can be expressed as

$$C_j(t) = A_j h(t - jT). \tag{8}$$

And $z_{\mathrm{ISI},j}(t)$ is the sum of the remaining molecular concentrations of the previous symbols. The ISI signal can be expressed here as

$$z_{\mathrm{ISI},j}(t) = \sum_{i=0}^{j-1} A_i h(t - iT), \quad jT < t \leq (j+1)T. \tag{9}$$

Additive counting noise is generated due to the random motion of the information molecules. From [31], the total noisy molecular concentration $z(t)$ is given by

$$z(t) = C_j(t) + z_{\mathrm{ISI},j}(t) + n(t), \tag{10}$$

where $n(t)$ is the non-stationary and signal-dependent additive noise. According to the definition of S_{O_2} in (1) we mentioned before, when 2,3-DPG molecules arrive at the receiver area, the blood oxygen saturation S_s can be expressed as

$$S_s = \frac{C_{HbO_2} - f(M,t)}{C_{HbO_2} + C_{Hb}}, \tag{11}$$

where $f(M,t)$ is the function which represents the decrease part in HbO_2 concentration after the release of 2,3-DPG. This function is related to both the molecular quantity M of the released 2,3-DPG and the current time t.

Reference [26] gives a clear derivation of the relationship between the concentration of 2,3-DPG and oxygen saturation, which is too complex. We consider another way to calculate it approximately. We adopt a model in [32] to calculate oxygen saturation. In [32], the equation for the ODC describes the oxygen saturation S_{O_2} as a function of oxygen partial pressure P_{O_2} relative to the half-saturation level P_{50}

$$S_{O_2} = \frac{(\frac{P_{O_2}}{P_{50}})^n}{1 + (\frac{P_{O_2}}{P_{50}})^n}, \tag{12}$$

where n is the Hill exponent. The value n = 2.7 was found to fit well to the data for normal human blood in the saturation range of 20–98%. According to [26], when pH = 7.24, P_{CO_2} = 40 mmHg, T = 37 °C, the relationship between P_{50} and 2,3-DPG concentration C can be calculated as

$$\begin{aligned} P_{50} = 26.8 &+ 795.63(C - 0.00465) \\ &- 19660.89(C - 0.00465)^2. \end{aligned} \tag{13}$$

From [33], P_{O_2} in arterial blood is around 90 mmHg. Thus, we can calculate the current S_{O_2} as long as we know the concentration of 2,3-DPG based on (12) and (13) when all other conditions are certain, providing a theoretical basis for the following calculation of mutual information quantities when calculating 2,3-DPG directly.

The output decoding can also be performed based on the general method of oximeter measurement. Two beams of light with different wavelengths (red light and infrared light) are used as the incident light in the measurement of blood oxygen saturation. According to [25], when the wavelength of the infrared light is taken near 805 nm, the blood oxygen saturation can be expressed as

$$S_{O_2} = A \times \frac{I_{AC}^{\lambda_1} / I_{DC}^{\lambda_1}}{I_{AC}^{\lambda_2} / I_{DC}^{\lambda_2}} - B, \tag{14}$$

where A and B are expressions about the absorption coefficient, which can generally be regarded as constants. $I_{AC}^{\lambda_1}$, $I_{AC}^{\lambda_2}$ are respectively the pulsatile component of transmitted light intensity when the light with a wavelength of λ_1 or λ_2 vertically enters the arterial blood of the fingertip of the human body. $I_{DC}^{\lambda_1}$, $I_{DC}^{\lambda_2}$ are respectively the non-pulsatile component of transmitted light intensity when the light with a wavelength of λ_1 or λ_2 vertically enters the venous blood of the fingertip of the human body. In this way, we can detect the oxygen saturation at the receiver as S_r. The decision equation of the receiver is

$$\hat{x} = \begin{cases} bit\text{“1”}, S_r \leq S_{th} \\ bit\text{“0”}, S_r > S_{th}, \end{cases} \tag{15}$$

where S_{th} is the receiver's decision threshold and $\hat{x}$ is recovered signal. In a time interval, if $S_r > S_{th}$ is detected, the bit received in this time period is considered to be 0. Otherwise, it is 1.

IV. Mutual Information for Proposed System

In this section, the mutual information of the designed communication system is derived and calculated.

In information theory, MI of two random variables is a measure of interdependence between two variables. More specifically, it measures the amount of information that can be obtained about one random variable by observing another random variable. From a system-wide perspective, MI represents the reduction in uncertainty of the entire system after communication. It measures the information shared between two random variables, X and Y. When the value of one random variable is known, it reduces the uncertainty of the other random variable. In a communication system, if we use X to represent the information sent by the transmitter and Y to represent the information received by the receiver, then MI between these two variables X and Y is closely related to the statistical characteristics of the channel in our constructed communication system.

We mentioned before that the blood oxygen saturation is measured by the optical detection method at the receiver. The receiver of the actual system should be outside the human body. Here, in order to calculate the number of 2,3-DPG

molecules in the blood vessel detected by the receiver, we assume a cylindrical receptive space with radius r, height h, and volume $V_R = \pi r^2 h$ is used to statistically calculate the number of molecules of 2,3-DPG. The purpose of using a cylindrical space is to characterize the number of 2,3-DPG molecules in the area where the light enters the blood vessel to make it more intuitive. In fact, the choice of the shape of the space does not make much difference to the simulation. Moreover, the concentration of molecules in this receptive space is uniform. This assumption is widely adopted in literature such as [34], [35]. So the number of noise-free molecules $N(t)$ received at the receiver can be expressed as

$$N(t) = y(t) \times V_R. \tag{16}$$

We have referred in section III that due to the random movement of information molecules, an additive counting noise is generated. The number of received molecules in the reception space affected by noise is represented by $\hat{N}(t)$, which follows a Poisson distribution [36]. The mean and variance of this random variable are both equal to $N(t)$. If we assume that $\hat{N}(t)$ is big enough, $\hat{N}(t)$ could be approximated as a normal distribution [31], i.e.,

$$\hat{N}(t) \sim \mathcal{N}\big(N(t), N(t)\big). \tag{17}$$

Thus the additive noise $n(t)$ follows a zero mean normal distribution $n(t) \sim \mathcal{N}[0, \frac{N(t)}{V_R^2}]$. With (16), we can further obtain

$$n(t) \sim \mathcal{N}[0, \frac{y(t)}{V_R}]. \tag{18}$$

This system is a static molecular communication system under the influence of blood flow rate, and its CIR is shown in (4). The probability of sending symbol "1" (event H_1) and symbol "0" (event H_0) is

$$\begin{aligned} p_1 &= P(H_1), \\ p_0 &= P(H_0). \end{aligned} \tag{19}$$

We assume that ISI mitigation techniques are used to fully mitigate the impact of ISI on the received signal [37], the expected peak concentration of the current symbol is expressed as

$$\begin{aligned} c_j^0 &= C_j^0(jT + t_{\text{peak}}) = A_0 h(t_{\text{peak}}), \\ c_j^1 &= C_j^1(jT + t_{\text{peak}}) = A_1 h(t_{\text{peak}}) \end{aligned} \tag{20}$$

for symbol "0" and symbol "1" respectively.

Here c_j^0 and c_j^1 are the average received peak concentrations of the jth symbol interval for symbol "0" and symbol "1" respectively. Same as in (8), $C_j^1(t)$ is the concentration of molecules received when the current jth symbol is 1, and $C_j^0(t)$ is the concentration of molecules received when the current jth symbol is 0.

As shown in (18), in order to calculate the signal-dependent noise variances σ_0 and σ_1, the expected received peak concentration is first calculated. The expected ISI amplitude of the ith symbol at peak time t_{peak} in the jth symbol interval is

$$z_{\text{ISI},j}^i = (p_0 A_0 + p_1 A_1) h[(j-i)T + t_{\text{peak}}]. \tag{21}$$

So the total ISI signal in the jth symbol interval can be expressed as

$$\begin{aligned} z_{\text{ISI},j} &= \sum_{i=0}^{j-1} z_{\text{ISI},j}^i \\ &= (p_0 A_0 + p_1 A_1) \sum_{i=0}^{j-1} h[(j-i)T + t_{\text{peak}}]. \end{aligned} \tag{22}$$

Although ISI is mitigated in the peak concentration, its contribution to noise cannot be simultaneously mitigated as discussed above. Then the noise variance of symbols "1" and "0" in jth symbol can be expressed as

$$\begin{aligned} (\sigma_j^0)^2 &= \frac{1}{V_R}(c_j^0 + z_{\text{ISI},j}) \\ &= \frac{p_1 M}{V_R} \sum_{i=0}^{j-1} h((j-i)T + t_{\text{peak}}), \\ (\sigma_j^1)^2 &= \frac{1}{V_R}(c_j^1 + z_{\text{ISI},j}) \\ &= \frac{1}{V_R}[Mh(t_{\text{peak}}) + p_1 M \sum_{i=0}^{j-1} h((j-i)T + t_{\text{peak}})], \end{aligned} \tag{23}$$

where σ_j^0 and σ_j^1 are the variances of the received peak concentrations of the jth symbol interval for symbol "0" and symbol "1" respectively.

Due to the fact that the transmitter and receiver are static in a static molecular communication scenario, the average peak concentration of the received symbols "0" and "1" does not vary depending on the time slot. This also means that c_j^0 and c_j^1 do not vary with j but maintain the same for different symbol intervals. Therefore, we define μ_0 and μ_1 as the average received peak concentrations of symbol "0" and symbol "1" respectively. Since we have adopted the OOK modulation method, A_0, A_1 in (20) can be represented by the value in (3), and then the average received peak concentrations of symbol "0" and symbol "1" can be expressed as

$$\begin{aligned} \mu_0 &= c_j^0 = 0, \\ \mu_1 &= c_j^1 = Mh(t_{\text{peak}}). \end{aligned} \tag{24}$$

We can clearly find that the distribution of signal molecules received by the receiver for the bit "0" obeys a Gaussian distribution with an average value of 0. But in theory, the receiver we use in practical applications cannot receive signal molecules with negative values. Although this problem can be easily solved by modifying the modulation method, this article uses the OOK modulation method, so we ignore this problem for the time being and still try to use the normal distribution to calculate MI when doing simulation.

We already mentioned that the transmitter and receiver are static in this communication scenario, so the noise variance of symbols "1" and "0" also does not vary with j. However, the results in (23) seem to contradict our proposed conclusions. But in fact, the farther the distance from the current jth symbol, the less the contribution to ISI, and the smaller the impact on the signal variance, so the distance from the current jth symbol is too far away and can be ignored. In the actual

simulation, we consider the current signal and ISI effect can last for q time slots. So the variance can be re-expressed as

$$(\sigma_0)^2 = \frac{p_1 M}{V_R}\sum_{i=0}^{q} h(iT + t_{\text{peak}}),$$
$$(\sigma_1)^2 = \frac{1}{V_R}[Mh(t_{\text{peak}}) + p_1 M\sum_{i=0}^{q} h(iT + t_{\text{peak}})]. \quad (25)$$

In Section III, we have already mentioned that the determination of blood oxygen saturation is achieved through optical detection methods. The relationship between the concentration of 2,3-DPG molecules at the receiver and blood oxygen saturation is determined, which can be approximated as an inversely proportional relationship. Therefore, we detect the signal by comparing the number of 2,3-DPG molecules received within the jth symbol interval (represented as y_j) with the threshold (represented as y_{th}). The symbols detected by the system receiver can be represented as

$$\hat{y} = \begin{cases} \text{bit“1”}, & y_j \geq y_{\text{th}} \\ \text{bit“0”}, & y_j < y_{\text{th}}. \end{cases} \quad (26)$$

The error probabilities of each symbol are

$$P_{xy}(1|0) = \int_{y_{\text{th}}}^{+\infty} \frac{1}{\sqrt{2\pi}\sigma_0}\exp\left[\frac{-(y-\mu_0)^2}{2\sigma_0^2}\right]dy$$
$$= Q\left(\frac{y_{\text{th}} - \mu_0}{\sigma_0}\right),$$
$$P_{xy}(0|1) = \int_{-\infty}^{y_{\text{th}}} \frac{1}{\sqrt{2\pi}\sigma_1}\exp\left[\frac{-(y-\mu_1)^2}{2\sigma_1^2}\right]dy$$
$$= 1 - Q\left(\frac{y_{\text{th}} - \mu_1}{\sigma_1}\right), \quad (27)$$

where $Q(\cdot)$ is the Q function.

Then the bit error probability of the entire communication system, denoted as P_e, can be expressed as

$$P_e = p_1 P_{xy}(0|1) + p_0 P_{xy}(1|0). \quad (28)$$

According to probability theory, we can further calculate the joint probability of X and Y, which can be expressed as

$$\begin{aligned} p(0,1) &= p_0 P_{xy}(1|0) \\ &= p_0 Q\left(\frac{y_{\text{th}} - \mu_0}{\sigma_0}\right), \\ p(1,0) &= p_1 P_{xy}\left(0|1\right)) \\ &= p_1[1 - Q\left(\frac{y_{\text{th}} - \mu_1}{\sigma_1}\right)], \\ p(0,0) &= p_0\big(1 - P_{xy}(1|0)\big) \\ &= p_0[1 - Q\left(\frac{y_{\text{th}} - \mu_0}{\sigma_0}\right)], \\ p(1,1) &= p_1\big(1 - P_{xy}(0|1)\big) \\ &= p_1 Q\left(\frac{y_{\text{th}} - \mu_1}{\sigma_1}\right). \end{aligned} \quad (29)$$

Next, we can calculate the marginal probabilities $p(x)$ and $p(y)$ by

$$\begin{aligned} p(x) &= p(x,0) + p(x,1), \\ p(y) &= p(0,y) + p(1,y). \end{aligned} \quad (30)$$

Then, we can calculate the MI by

$$I(X;Y) = \sum_{y\in Y}\sum_{x\in X} p(x,y)\log\frac{p(x,y)}{p(x)p(y)}, \quad (31)$$

where X is the random variable at the transmitter, and Y is the random variable at the receiver in our system.

V. Stimulation Results

In this section, the bit error rate (BER) and MI of the through-body communication system are evaluated by MATLAB. The impacts of several important parameters such as distance between the nanomachine and the receiver, blood flow velocity, and decision threshold on BER in our communication system are investigated. In addition, the impact of the above parameters, symbol probability, and the number of released molecules on MI is further analyzed and discussed.

On the selection of the parameter range, the distance between the nanomachine and receiver is chosen from 8 mm to 12 mm since the distance between the middle transverse palmar branch and the distal transverse palmar branch is about 10.33 mm [38]. Considering that the reasonable range of the blood flow velocity is from 30 mm/s to 126 mm/s [39], we set the velocity from 60 mm/s to 100 mm/s. The molecular diffusion coefficient is set as 200 mm^2/s. As for the setting of the receptive space, we chose a cylinder with a radius of 1mm and a height of 1.5mm [41]. Table I shows some important parameters used in the simulation.

The relationship of decision threshold, the distance between the nanomachine and the receiver, and BER is shown in Fig. 2. Here, we define M in (3) as 50000 when the nanomachine sends the symbol “1”. Symbol interval is chosen as 1 ms. The probability that the transmitter sends symbol “1” and symbol “0” are the same, both are 0.5. In this simulation, the blood flow velocity was set as 80 mm/s. It can be seen from the figure that the selection of the decision threshold has a great influence on the performance of the whole system. When other parameters are stable, there is an optimal decision threshold in the graph, which can minimize the error probability of the system. Correspondingly, the distance between the nanomachine and the receiver determines the minimum level limit of the system bit error rate. The relationship of MI to the threshold is also investigated which is shown in Fig. 3. It shows the opposite trend to the error probability curve. When the appropriate threshold is selected, the error probability decreases whereas the MI increases with respect to the decrease of the distance between the nanomachine and the receiver.

Fig. 4 and Fig. 5 show the relationship between decision threshold and BER and MI with different blood flow velocities. In this simulation, the distance between the nanomachine and the receiver is set to 10 mm. Except for the blood flow velocity and distance, the rest of the simulation parameters are the same as the above simulation. Similar to what is shown in the previous figure, when other parameters are stable, there is also an optimal decision threshold, which can minimize the error probability of the system and maximize the MI of the system. The blood flow velocity determines the minimum level limit of BER and the maximum level limit of MI. In this process,

TABLE I
STIMULATION PARAMETERS

Parameters	Symbol	Value
Distance between nanomachine and receiver	d	8-12 mm [38]
Blood flow velocity	v	60-100 mm/s [39]
Diffusion coefficient	D	200 mm^2/s [40]
Number of 2,3-DPG molecules	M	10000-50000
Radius of the receptive space	r	1 mm [41]
Height of the receptive space	h	1.5 mm [41]
Decision threshold	y_{th}	0-15
Symbol interval	T	1 ms
Symbol probability of bit "1"	p_1	0.1-0.9

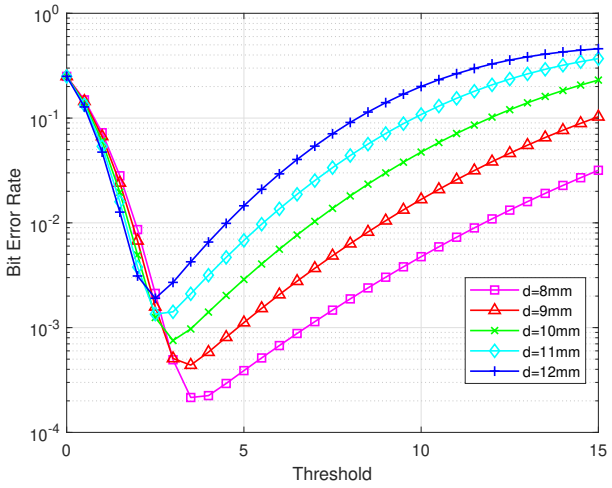

Fig. 2. The relationship of the BER and the decision threshold for different distances between nanomachine and receiver.

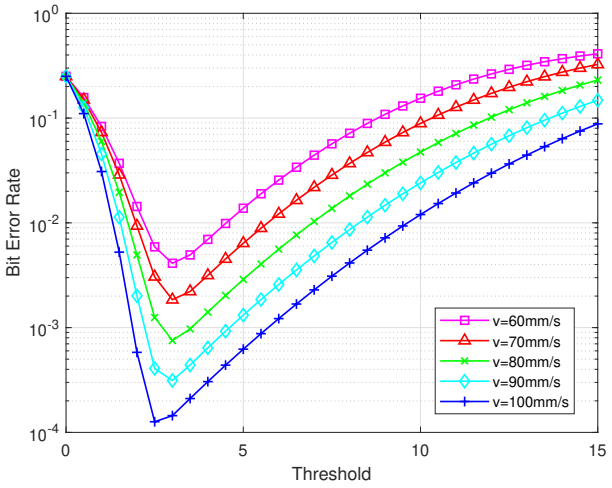

Fig. 4. The relationship of the BER and the decision threshold for different blood flow velocities.

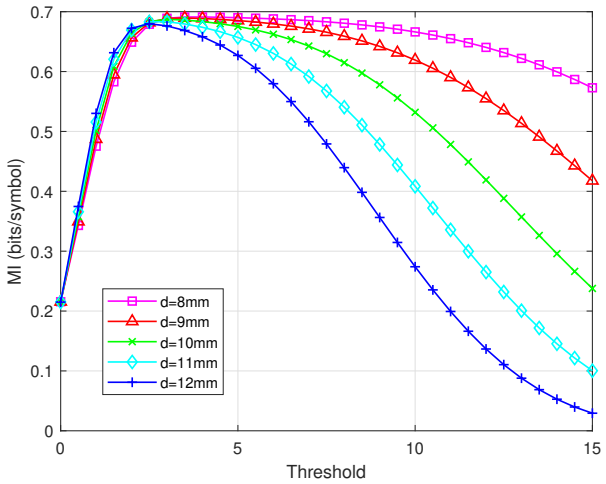

Fig. 3. The relationship of the MI and the decision threshold for different distances between nanomachine and receiver.

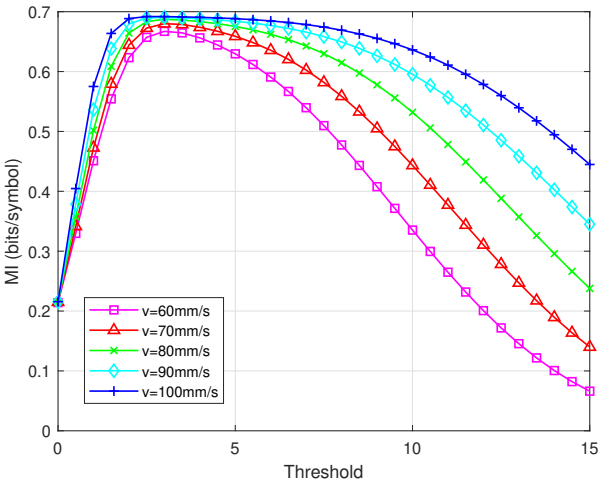

Fig. 5. The relationship of the MI and the decision threshold for different blood flow velocities.

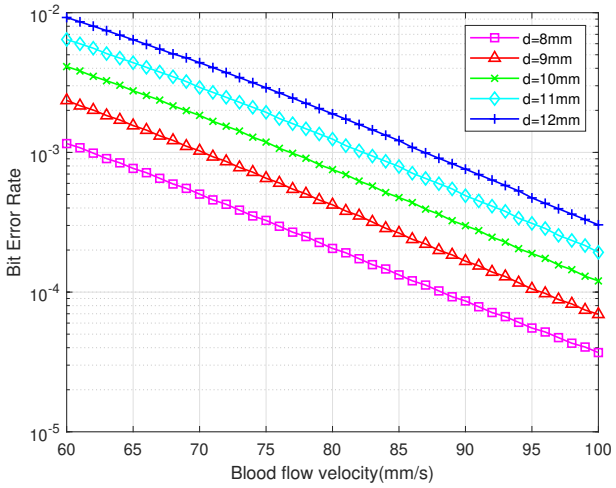

Fig. 6. The relationship of BER and blood flow velocity for different distances between nanomachine and receiver.

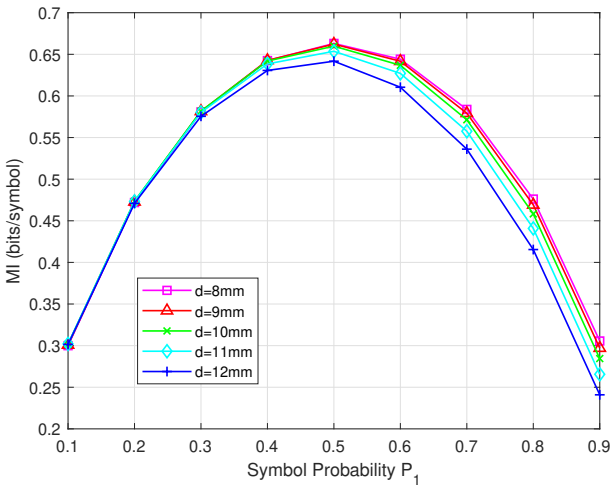

Fig. 8. The relationship of the MI and the symbol probability for different distances between nanomachine and receiver.

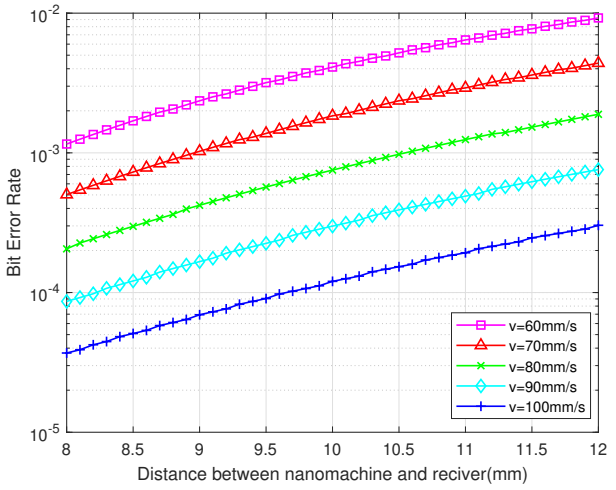

Fig. 7. The relationship of the BER and the distance between nanomachine and receiver for different blood flow velocities.

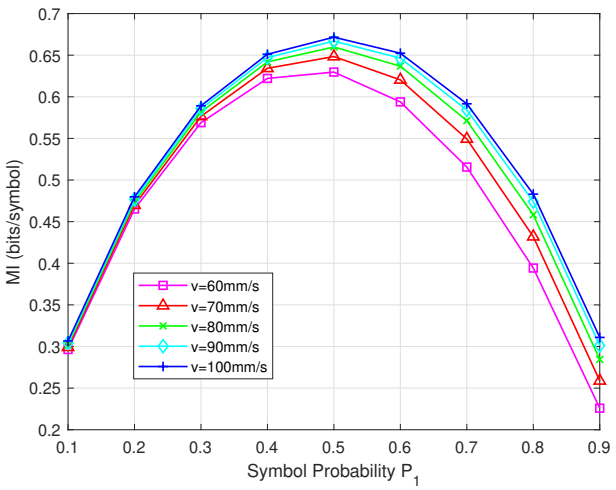

Fig. 9. The relationship of the MI and the symbol probability for different blood flow velocities.

BER decreases with increasing blood flow velocity, while MI increases with increasing blood flow velocity.

From the above simulations, it is not difficult to see that the selection of the decision threshold is very important to the entire simulation process. So in all the following simulation tests, the decision thresholds we choose are calculated based on other parameters in the current simulation to minimize the system BER. This process can be achieved by giving the system receiver different decision thresholds and calculating the minimum value of BER when other parameters are certain.

After determining the decision threshold, the relationship between BER and blood flow velocity is shown in Fig. 6. It can be seen that as the increase of velocity v, the BER decreases. This is because the increase of v leads to a larger peak value in (5). It also speeds up the concentration decay to reduce the influence of the long tail effect of signal molecules when 2,3-DPG molecules diffuse. Therefore, the ISI effect is reduced in this process and more molecules will be received at the receiver. It can also be seen that as the increase of distance d, BER decreases in Fig. 7. Similar to the discussion process for v, the increase of d leads to a smaller peak value $C(t)$, and further less 2,3-DPG molecules arriving at the receiver.

In Fig. 8 and Fig. 9, the impact of symbol probability, blood flow velocity, and the distance between the nanomachine and the receiver on the MI is investigated. It is not difficult to find that MI first increases and then decreases with the increase of symbol probability p_1, and when $p_1 = p_0 = 0.5$, MI takes the maximum value. It is obvious in Fig. 8 that the MI increases as the distance decreases. In Fig. 9, we can find that the MI increases as the velocity increases. There is another obvious thing that the MI curve is not symmetric about $p_1 = 0.5$. For example, for all five curves in Fig. 9, MI at $p_1 = 0.1$ is larger than that at $p_1 = 0.9$ when the blood flow velocity is relatively low. But as the speed increases, the MI at $p_1 = 0.9$ finally exceeds that at $p_1 = 0.1$. The change of speed will have a greater impact on μ_1 and σ_1 but has less impact on σ_0, and no

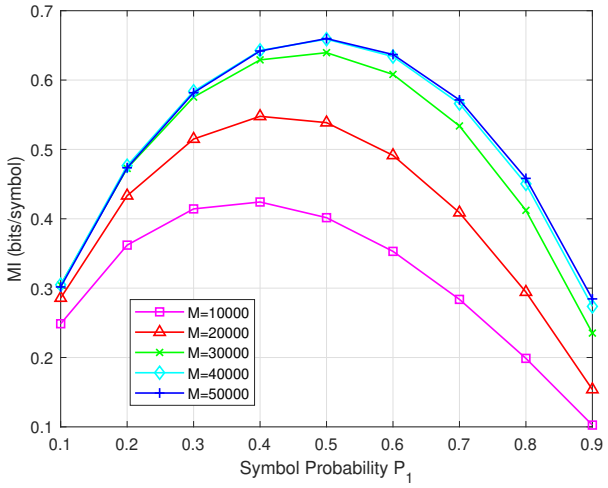

Fig. 10. The relationship of the MI and the symbol probability for different numbers of 2,3-DPG molecules nanomachine released for symbol "1".

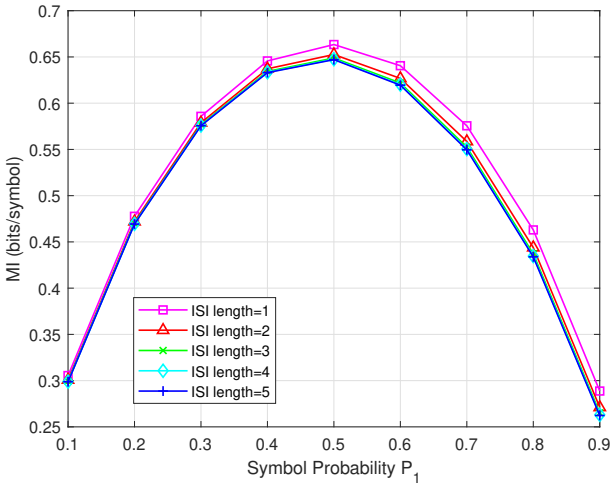

Fig. 11. The relationship of the MI and the symbol probability with different ISI lengths.

impact on μ_0. When the probability of p_1 is high, this process will also affect MI to a greater extent, making $P_{xy}(0|1) < P_{xy}(1|0)$ gradually become $P_{xy}(0|1) > P_{xy}(1|0)$.

Fig. 10 shows the influence of symbol probability p_1 and the number of 2,3-DPG molecules nanomachine released for symbol "1" on MI. It can be clearly seen that as the number of released molecules increases, MI also increases. When the number of released molecules increases to a certain extent, MI basically remains unchanged. This is because when the number of released molecules is small, the number of molecules arriving at the receiver is also small, and the selection of the judgment threshold is highly demanding, which is prone to misjudgment. When the number of released molecules increases, the distance between μ_0 and μ_1 increases, the probability of misjudgment decreases, and MI increases.

The impact of symbol probability and ISI effect are investigated and the result is shown in Fig. 11. It can be seen that considering the ISI effect, the longer the ISI length, the smaller the MI. This is easy to understand because ISI increases the noise variance. Even if the ISI is completely eliminated after the fact through the ISI mitigation method, its influence on the noise cannot be eliminated. Increased noise variance increases BER and reduces mutual information.

VI. Conclusion

In this paper, we propose a novel communication system between a nanonetwork consisting of biosensors inside the human blood vessels and outside the human body. The nanomachine acts as the transmitter in the blood vessel, sending signals by releasing 2,3-DPG to alter the blood oxygen saturation. The outside receiver detects the blood oxygen saturation by optical technology to make decisions. The framework of the whole communication system is presented and mathematically modeled. We calculate and simulate the bit error rate and mutual information of the proposed model, and discuss the influence of various important parameters such as decision threshold, blood flow velocity, and simulation of transmitting and receiving distances on the bit error rate and mutual information. This study is an exploration of the through-body communication system for the principle of optical detection. In our future work, we will conduct practical experimental tests of this system design and consider experiments in live animals. In addition, we are also considering further improvements to the current 3-D advection-diffusion model by using a more refined model of molecular diffusion in blood vessels.

References

[1] L. Lin, F. Huang, H. Yan, F. Liu, and W. Guo, "Ant-behavior inspired intelligent nanonet for targeted drug delivery in cancer therapy," *IEEE Trans. Nanobiosci.*, vol. 19, no. 3, pp. 323–332, 2020.

[2] Y. Zhang, F. Huang, J. Song, L. Lin, Y. Yang, X. Zhi, and H. Yan, "Hardware verification of a micro-scale receiver for synthetic dna molecular communications," *IEEE Trans. Mol. Biol. Multi-Scale Commun.*, 2023.

[3] L. Kong, L. Huang, L. Lin, Z. Zheng, Y. Li, Q. Wang, and G. Liu, "A survey for possible technologies of micro/nanomachines used for molecular communication within 6g application scenarios," *IEEE Internet Things J.*, vol. 10, no. 13, pp. 11 240–11 263, 2023.

[4] R. Noormohammadi, A. Khaleghi, and I. Balasingham, "Galvanic impulse wireless communication for biomedical implants," *IEEE Access*, vol. 9, pp. 38 602–38 610, 2021.

[5] C. Zhang, Q. Jin, M. Zhao, D. Zhang, and L. Lin, "An experimental study of digital communication system with human body as communication channel," in *Proc. 2022 IEEE-EMBS Int. Conf. Wearable Implant. Body Sensor Netw. (BSN)*. IEEE, 2022, pp. 1–4.

[6] Y. Li, L. Lin, W. Guo, D. Zhang, and K. Yang, "Error performance and mutual information for IONT interface system," *IEEE Internet Things J.*, vol. 9, no. 12, pp. 9831–9842, 2022.

[7] L. Lin, L. Huang, L. Kong, F. Liu, and H. Yan, "Review of recent advancement of molecular communication," *Acta Electron. Sin.*, vol. 50, no. 6, p. 1492, 2022.

[8] S. A. Abdel Hakeem, H. H. Hussein, and H. Kim, "Security requirements and challenges of 6g technologies and applications," *Sensors*, vol. 22, no. 5, p. 1969, 2022.

[9] F. Calì, L. Fichera, G. T. Sfrazzetto, G. Nicotra, G. Sfuncia, E. Bruno, L. Lanzanò, I. Barbagallo, G. Li-Destri, and N. Tuccitto, "Fluorescent nanoparticles for reliable communication among implantable medical devices," *Carbon*, vol. 190, pp. 262–275, 2022.

[10] P. G. Jamkhande, N. W. Ghule, A. H. Bamer, and M. G. Kalaskar, "Metal nanoparticles synthesis: An overview on methods of preparation, advantages and disadvantages, and applications," *J. Drug Deliv. Sci. Technol.*, vol. 53, p. 101174, 2019.

[11] Y. Dong, L. Wang, V. Iacovacci, X. Wang, L. Zhang, and B. J. Nelson, "Magnetic helical micro-/nanomachines: Recent progress and perspective," *Matter*, vol. 5, no. 1, pp. 77–109, 2022.

[12] J. Ouyang, L. Sun, F. Zeng, and S. Wu, "Biomarker-activatable probes based on smart aiegens for fluorescence and optoacoustic imaging," *Coord. Chem. Rev.*, vol. 458, p. 214438, 2022.

[13] L. Felicetti, M. Femminella, G. Reali, and P. Liò, "A molecular communication system in blood vessels for tumor detection," in *Proc. ACM 1st Annu. Int. Conf. Nanoscale Comput. Commun.*, 2014, pp. 1–9.

[14] W. Wang, W. Yu, H. Yan, and L. Lin, "An experimental platform for molecular communication based on light absorption," in *IEEE 23rd Int. Conf. Nanotechnol.* IEEE, 2023, pp. 882–887.

[15] A. Cheung, L. Tu, A. Macnab, B. K. Kwon, and B. Shadgan, "Detection of hypoxia by near-infrared spectroscopy and pulse oximetry: a comparative study," *J. Biomed. Opt.*, vol. 27, no. 7, p. 077001, 2022.

[16] W. Zhong, Z. Ji, and C. Sun, "A review of monitoring methods for cerebral blood oxygen saturation," in *Healthcare*, vol. 9, no. 9. MDPI, 2021, p. 1104.

[17] E. Vavrinsky, N. E. Esfahani, M. Hausner, A. Kuzma, V. Rezo, M. Donoval, and H. Kosnacova, "The current state of optical sensors in medical wearables," *Biosensors*, vol. 12, no. 4, p. 217, 2022.

[18] C. Zhang, H. Yan, Q. Liu, K. Yang, and L. Lin, "Signal transmission through human body via human oxygen saturation detection," in *International Conference on Bio-inspired Information and Communication Technologies*. Springer, 2023, pp. 190–199.

[19] J. Toffaletti and W. G. Zijlstra, "Misconceptions in reporting oxygen saturation," *Anesth. Analg.*, vol. 105, no. 6, pp. S5–S9, 2007.

[20] J.-A. Collins, A. Rudenski, J. Gibson, L. Howard, and R. O'Driscoll, "Relating oxygen partial pressure, saturation and content: the haemoglobin–oxygen dissociation curve," *Breathe*, vol. 11, no. 3, pp. 194–201, 2015.

[21] T. Walsh and E.-E.-D. Saleh, "Anaemia during critical illness," *Br. J. Anaesth.*, vol. 97, no. 3, pp. 278–291, 2006.

[22] P. A. Kyriacou, "Introduction to photoplethysmography," in *Photoplethysmography*. Elsevier, 2022, pp. 1–16.

[23] C. M. Alexander, L. E. Teller, and J. B. Gross, "Principles of pulse oximetry: theoretical and practical considerations," *Anesth. Analg.*, vol. 68, no. 3, pp. 368–376, 1989.

[24] E. D. Chan, M. M. Chan, and M. M. Chan, "Pulse oximetry: understanding its basic principles facilitates appreciation of its limitations," *Respir. Med.*, vol. 107, no. 6, pp. 789–799, 2013.

[25] Z. Luo, S. Zhang, and Y. Yang, *Engineering Analysis and Clinical Applications of Pulse Wave*. Science Press, 2006.

[26] R. K. Dash and J. B. Bassingthwaighte, "Erratum to: Blood $\mathrm{HbO_2}$ and $\mathrm{HbCO_2}$ dissociation curves at varied $\mathrm{O_2}$, $\mathrm{CO_2}$, pH, 2, 3-DPG and temperature levels," *Ann. Biomed. Eng.*, vol. 38, no. 4, pp. 1683–1701, 2010.

[27] A. H. Schmaier and H. M. Lazarus, *Concise guide to hematology*. John Wiley & Sons, 2011.

[28] J. Toffaletti and C. Rackley, "Monitoring oxygen status," *Advan. Clin. Chem.*, vol. 77, pp. 103–124, 2016.

[29] P. van Es, S. K. Biswas, H. J. B. Moens, W. Steenbergen, and S. Manohar, "Initial results of finger imaging using photoacoustic computed tomography," *J. Biomed. Opt.*, vol. 19, no. 6, pp. 060 501–060 501, 2014.

[30] N. Farsad, H. B. Yilmaz, A. Eckford, C.-B. Chae, and W. Guo, "A comprehensive survey of recent advancements in molecular communication," *IEEE Commun. Surv. Tutor.*, vol. 18, no. 3, pp. 1887–1919, 2016.

[31] L. Lin, Q. Wu, F. Liu, and H. Yan, "Mutual information and maximum achievable rate for mobile molecular communication systems," *IEEE Trans. Nanobiosci.*, vol. 17, no. 4, pp. 507–517, 2018.

[32] A. V. Hill, "The possible effects of the aggregation of the molecules of hemoglobin on its dissociation curves," *J. Physiol.*, vol. 40, pp. iv–vii, 1910.

[33] E. Ortiz-Prado, J. F. Dunn, J. Vasconez, D. Castillo, and G. Viscor, "Partial pressure of oxygen in the human body: a general review," *Am. J. Blood Res.*, vol. 9, no. 1, p. 1, 2019.

[34] L.-S. Meng, P.-C. Yeh, K.-C. Chen, and I. F. Akyildiz, "On receiver design for diffusion-based molecular communication," *IEEE Trans. Signal Process.*, vol. 62, no. 22, pp. 6032–6044, 2014.

[35] M. Pierobon and I. F. Akyildiz, "Diffusion-based noise analysis for molecular communication in nanonetworks," *IEEE Trans. Signal Process.*, vol. 59, no. 6, pp. 2532–2547, 2011.

[36] D. Kilinc and O. B. Akan, "Receiver design for molecular communication," *IEEE J. Sel. Areas Commun.*, vol. 31, no. 12, pp. 705–714, 2013.

[37] G. Chang, L. Lin, and H. Yan, "Adaptive detection and ISI mitigation for mobile molecular communication," *IEEE Trans. Nanobiosci.*, vol. 17, no. 1, pp. 21–35, 2017.

[38] C. Lihua, H. Hongtai, H. Qunwu, H. Zhengrui, and L. Wenchao, "Applied anatomy of proper digital palmar artery," *Chinese J. Anat.*, vol. 29, no. 4, pp. 503–505, 2006.

[39] F. Yusheng, Q. Wang, J. Yi, D. Song, and X. Xiang, "A numerical model of blood flow velocity measurement based on finger ring," *J. Healthc. Eng.*, vol. 2018, 2018.

[40] L. P. Giné and I. F. Akyildiz, "Molecular communication options for long range nanonetworks," *Comput. Netw.*, vol. 53, no. 16, pp. 2753–2766, 2009.

[41] S. Chatterjee and P. A. Kyriacou, "Monte carlo analysis of optical interactions in reflectance and transmittance finger photoplethysmography," *Sensors*, vol. 19, no. 4, p. 789, 2019.

Chengyi Zhang (Graduate Student Member, IEEE) received the B.S. degree in electronic information engineering from Tongji University, Shanghai, China, in 2022. He is currently pursuing the M.S. degree with Tongji University. His research interests include molecular communication, neural communication, and Internet of Nanothings.

Hao Yan received the B.Eng. and M.Eng. degrees in electrical engineering from Tianjin University, China, in 2005 and 2007, respectively, and the Ph.D. degree from Nanyang Technological University, Singapore, in 2012. She is currently an Associate Professor with the School of Electronic, Information and Electrical Engineering, Shanghai Jiao Tong University, Shanghai, China. Her research interests include DNA molecular communications and Internet of Nanothings.

Qiang Liu received his B. S. (1996), M. S. (2000) and Ph.D. (2012) degrees from University of Electronic Science and Technology of China (UESTC) respectively. After graduating from M.S. study in 2000, he has worked with School of Communication and Information Engineering, UESTC, China, and is a professor now. He had worked in the University of Essex in U.K. (2012.12-2013.12) and the University of California, Davis in U.S.A (2017.8-2018.8) as a visitor scholar. His researches focus on wireless sensor networks, Internet of Things, broadband wireless networks and molecular communication. He is the member of IEEE. He is the reviewer of IEEE Transactions on NanoBioscience, International Journal of Communication Systems (IJCS) etc.

Kun Yang (F'23) received his PhD from the Department of Electronic & Electrical Engineering of University College London (UCL), UK. He is currently a Chair Professor in the School of Computer Science & Electronic Engineering, University of Essex, UK, leading the Network Convergence Laboratory (NCL). He is also an affiliated professor of Nanjing University, China. His main research interests include wireless networks and communications, future Internet and edge computing. In particular he is interested in energy aspects of future communication systems such as 6G, promoting energy self-sustainability via both energy efficiency (green communications and networks) and energy harvesting (wireless charging). He has managed research projects funded by UK EPSRC, EU FP7/H2020, and industries. He has published 400+ papers and filed 30 patents. He serves on the editorial boards of a number of IEEE journals (e.g., IEEE TNSE, TVT, WCL). He is a Deputy Editor-in-Chief of IET Smart Cities Journal. He has been a Judge of GSMA GLOMO Award at World Mobile Congress – Barcelona since 2019. He was a Distinguished Lecturer of IEEE ComSoc (2020-2021). He is a Member of Academia Europaea (MAE), a Fellow of IEEE, a Fellow of IET and a Distinguished Member of ACM.

Fuqiang Liu (Member, IEEE) received the bachelor's degree from Tianjin University, Tianjin, China, in 1987 and the Ph.D. degree from the China University of Mining and Technology, Xuzhou, China, in 1996. He is currently a Professor with the School of Electronics and Information Engineering, Tongji University, Shanghai, China, where he is currently the Director of the Broadband Wireless Communication and Multimedia Laboratory. He has authored or coauthored more than 300 scientific papers and nine books. His research interests mainly include theories and technologies of broadband wireless communications (fifth-generation mobile communications and vehicular communications/dedicated short-range communications) and their applications in automotive and intelligent transportation systems. Dr. Liu has participated in numerous national research projects in China and has received research funding from the United States, Finland, the European Union, and Japan.

Lin Lin (Senior Member, IEEE) received B.Eng. and M.Eng. degrees in electrical engineering from Tianjin University, China in 2004 and 2007, respectively, and the Ph.D. degree from Nanyang Technological University, Singapore in 2012. He is an Associate Professor with the College of Electronics and Information Engineering, Tongji University, Shanghai, China. He is currently the Chair of IEEE ComSoc Molecular, Biological and Multi-scale Communications Technical Committee, and the Chair of IEEE Nanotechnology Council Nanoscale Communications Technical Committee. He serves as Associate Editor for IEEE Transactions on Molecular, Biological and Multi-scale Communications, IEEE Nanotechnology Magazine, and IEEE Access. His research interests include molecular communications, neural communications, internet of nanothings, and body sensor networks. His research interests include molecular communication, neural communication, and Internet of Nanothings.